Detecting Nanohertz-Frequency Gravitational Waves using the MeerKAT Pulsar Timing Array

Matthew Bailes, Chris Flynn, Hendrik Combrinck†, Rudra Sekhri†, Rebecca Koehne†, Ruoyao Ni†, Evie Spilias†

Swinburne University of Technology, OzGrav, John Street, Melbourne, 3122, Victoria, Australia.

Contributing authors: mbailes@swin.edu.au; cflynn@swin.edu.au;
†These authors contributed equally to this work

Abstract

Pulsar timing arrays (PTAs) offer a new method to detect nano-hertz gravitational waves through a spatial correlation between the times of arrivals (ToAs) between pairs of pulsars. We report a detection of nHz gravitational waves with an estimated detection significance of approx $\boldsymbol{7\sigma}$ using the Karoo Array Telescope (MeerKAT) PTA project. An earlier analysis retrieved a significance of $\boldsymbol{\sim 5.85\sigma}$. Our re-analysis used a sample of 8387 observations from 83 millisecond pulsars (MSPs) over the course of 4 years, with a signal amplitude of $\boldsymbol{A = 5 \times 10^{-15}}$.

Keywords: Gravitational Wave Astronomy — Pulsar Timing Array — Radio Astronomy — Millisecond pulsars

1 Introduction

First described by Albert Einstein [8] and indirectly confirmed by Hulse, Taylor and collaborators [11] [24], gravitational waves (GWs) form from the acceleration of objects with mass. This was first confirmed through observation by the LIGO collaboration through the inspiral of a binary black hole system [1]. There has been a growing catalog of GW events, with the most recent being the third Gravitational-Wave Transient Catalog (GWTC-3) [2]. The gravitational wave events discovered by the LIGO collaboration typically have frequencies ranging from $\sim 10^1 - 10^3$ Hz.

PTAs typically involve multiple millisecond pulsars (MSPs), which are monitored

Table 1: A list of the amplitudes of Hellings and Downs correlations determined by other PTAs [22] [3] [4] [7], as well the corresponding detection significances for each study. Start and end years for each dataset used have also been provided. This is in comparison to the MeerKAT PTA dataset that has been used in this paper.

PTA	GWB amplitude	Significance σ	Pulsars	Start Year	End Year
Parkes PTA	$3.1^{1.3}_{-0.9} \times 10^{-15}$	$\sim 2\sigma$	30	2004	2021
NANOGrav PTA	$2.4^{+0.7}_{-0.6} \times 10^{-15}$	$3.5 - 4\sigma$	67	2004	2020
International PTA	$3.8^{+6.3}_{-2.5} \times 10^{-15}$	$\geq 3\sigma$	65	N/A	N/A
European PTA	$2.5^{+0.7}_{-0.7} \times 10^{-15}$	$\geq 3\sigma$	25	1996	2021
MeerKAT PTA	5×10^{-15}	$\sim 7\sigma$	83	2019	2023

every few days over the timescales of decades [9]. The sensitivity of a PTA to a gravitational wave source is dependent on the number of pulsars present in the PTA. There has been a growing effort [5] in pulsar astronomy to detect longer frequency gravitational waves ($\sim 10^{-9}$ Hz), which originate from much heavier mass binary systems. These binary systems typically consist of black holes of masses $\sim 10^5 - 10^{10} M_\odot$ [18] [16], and these black holes are typically found in the center of galaxies .

Galaxy mergers lead the formation of supermassive black hole (SMBH) binaries in the centres of active galactic nuclei (AGN) [15] [6], and these SMBH binaries emit low-frequency ($\sim 10^{-9}$ Hz) GWs over time. [13]. These low-frequency signals can be detected through PTAs. A signal with an amplitude as weak as 5×10^{-17} could be detected with 20 millisecond pulsars (MSPs), observing each pulsar once every two weeks for 5 yr with a timing accuracy of 15 ns [13].

Gravitational waves passing through affect the observed times of arrival (ToAs) from each MSP [23], leaving a correlated signal as a function of the angular separation on the sky of the pulsar pairs. This unique characteristic, called the Hellings- Downs correlation [10], confirms the detection of a nanohertz gravitational wave signal in the PTA dataset, and is noted as the "*signature*" of any gravitational wave background [22].

Previous studies using the Parkes Pulsar Timing Array (PPTA) [22] and the Nanohertz Gravitational Wave Collaboration (NanoGRAV) [3] report a $\sim 2.5\sigma - 4\sigma$ result in the detect of such a Hellings and Downs correlation from 18 years and 15 years of ToA data respectively. As of 2024, MeerKAT's ToA data extends back to 2019 and uses a set of 85 MSPs compared to PPTA's 30 MSPs and NanoGRAV's 67 pulsars.

2 Method

2.1 Original Data Acquisition

The analysis presented started with an extended version MeerKAT Data Release 1 [17] that extends to 2023, which includes pulsar times of arrival (ToA) data from 85 pulsars as part of the MeerKAT pulsar timing array (PTA) project. In total, this dataset includes 4 years of data, ranging from 2019 to 2023.

The analysis utilised data collected using the MeerKAT L-band (856–1712 MHz) receiver, with a central frequency of 1284 MHz [17], with each observation consisting of 1024 channels. These channels were grouped into 16 and 32 sub-band formats. The final Hellings-Downs correlation presented uses 32 band arrival times from MeerKAT.

2.2 Data Reduction Process

Both datasets were cleaned using objectively defined criteria, in order to optimise the search for sub-microsecond fluctuations in timing residuals caused by the presence of nanohertz gravitational waves, and to determine a correlated signal present within the MeerKAT PTA dataset. As such, arrival times with small uncertainties and high signal-to-noise ratios (SNRs) are selected from the entire dataset.

2.2.1 16-Band ToA Data

The 16-band arrival times are manually inspected to determine the best arrival time error cutoff for each pulsar as well as any bad observational epochs. These bad observational epochs are typically between 20 μs and 100 μs off the zero-point, usually multiple σ away. This was to ensure the reliability of the cleaned dataset. Some bad observational epochs applied to all pulsars, while others only applied to a small fraction of them.

For all 16 band arrival times, the signal-to-noise ratio (SNR) cutoff is set to 8, while the arrival time error cutoff is set to different amounts for each pulsar. A list of these parameters can be found in (appendix number).

PSR J1705−1903 was identified to have a black widow companion [14], with high fluctuations ($\sim 10 - 30\,\mu s$) in the arrival times. Due to the imprecision in timing residuals from the pulsar, it was deemed unsuitable for detecting sub-microsecond signals, and was hence discarded from the pulsar list.

PSR J0437−4715's arrival times had different numbers of channels for different observations. Some had 1024 channels while others had 4096 channels. Observations with 4096 channels were used to observe scintillation patterns induced by the interstellar medium [21] [19] and require high frequency resolution. PSR J0437−4715 is a bright MSP [12] and it suitable for such a scientific purpose. Therefore, this high frequency resolution observing mode (with 4096 channels) was used on this pulsar [20]. This different observing mode could have different systematics compared to the

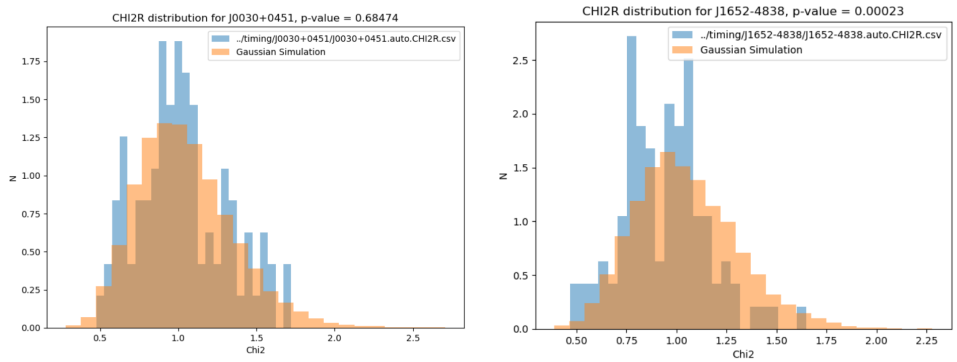

(a) J0030+0451 (b) J1652−4838

Fig. 1: The χ^2 distributions for two pulsars, PSR J0030+0451 and PSR J1652−4838 (blue) compared to the modelled χ^2 distribution from a Gaussian sample. The p-value is determined through the Komolgorov-Smirnov test.

1024-channel observing mode. This is why all high frequency resolution data for PSR J0437−4715 was not used in the analysis.

After this initial reduction process and the removal of PSR J1705−1903, 84 of the 85 pulsars remained. 34836 arrival times were discarded based on the criteria from the total of 115420. The percentage removed was 30.2 %. From the original total of 8397 observations for the 84 pulsars (excluding J1705−1903), 8387 remained.

2.2.2 32-Band Data

The 32 band arrival times are cleaned based on the epochs that were obtained from the 16 channel data, as these epochs are known to be multiple σ away from the zero-point. A minimum SNR was set to 6, a maximum arrival time error was set to 10, and a minimum observation length requirement of 128.0 s was applied to all pulsars. The data was culled based on observation length to limit the effect of jitter in each observation, and hence ensure reliability in each of the arrival times for each observation.

Similar to the 16 sub-band data, PSR J1705−1903 was removed, as well as high frequency resolution arrival time data for PSR J0437−4715.

Some timing residual datasets for pulsars were observed to have pairs of observations several microseconds ($\sim 5 - 10\,\mu s$) away from the zero-point, and separated by 1 s. These were identified to be experimentation of a new observing mode being calibrated on MeerKAT where two computers simultaneously process timing data from the telescope, and introduced previously unnoticed systematics to those observations. These were also removed.

The χ^2 value was calculated for each observation for each pulsar. We compared the distribution of χ^2 for each observation for each pulsar to the expected distribution of χ^2 using a Gaussian simulated dataset. Using the Kolmogorov-Smirnov test, the p-value was determined for each pulsar's χ^2 distribution to determine whether any systematic biases were present in the ToA dataset. Pulsars with p-values less than 0.2 ($p_{PSR} < 0.2$) were inspected and a list of observations with high χ^2 was compiled.

206 out of the cleaned total of 8387 observations had high χ^2 ($\chi^2 > 3.0$), and were inspected to determine the cause for this high result. Some were because of outliers (greater than 3σ away from the zero-point) still present in the dataset, leading to high χ^2 for those observations. These were removed to produce timing residuals with a lower χ^2 than before.

Corrected observations that still had a $\chi^2 > 3.6$ were removed. Observations with fewer than 5 sub-bands ($n_{bands} < 5$) were also removed to improve the quality of the DM fitting later in the process. Out of the 206 observations with high χ^2, 15 were removed. This is in comparison to the original cleaned dataset (prior to the χ^2 cleaning process) of 8387 observations.

2.3 Frequency Dependent Corrections

2.3.1 16-band Data

During the fitting process of the 16 band arrival times, no frequency dependent (FD) parameters were used. We use these cleaned, fitted timing residuals to inspect for FD structures within the ToAs for each pulsar.

The majority of pulsars exhibited some FD structure, and this is due to out-of-date template profiles for each pulsar for 16 frequency bands, which results in FD structures. As such, FD corrections were applied to each respective channel for each pulsar to account for bad pulse template profiles. A list of each of the corrections applied to each of the 16 frequency bands for each pulsar is provided in appendix ().

The FD corrections applied are the weighted mean timing residual zero-point offsets for each of the 16 frequency bands, which are subtracted from the arrival times to construct a new, FD corrected ToA dataset.

2.3.2 32 band data

No FD corrections were applied to the 32 band timing residuals. Neither were frequency dependent parameters used during the fitting process for each of the ToA datasets. This is due to new timing profiles for 32-band data, leading to no significant FD structures in the timing residuals for each pulsar.

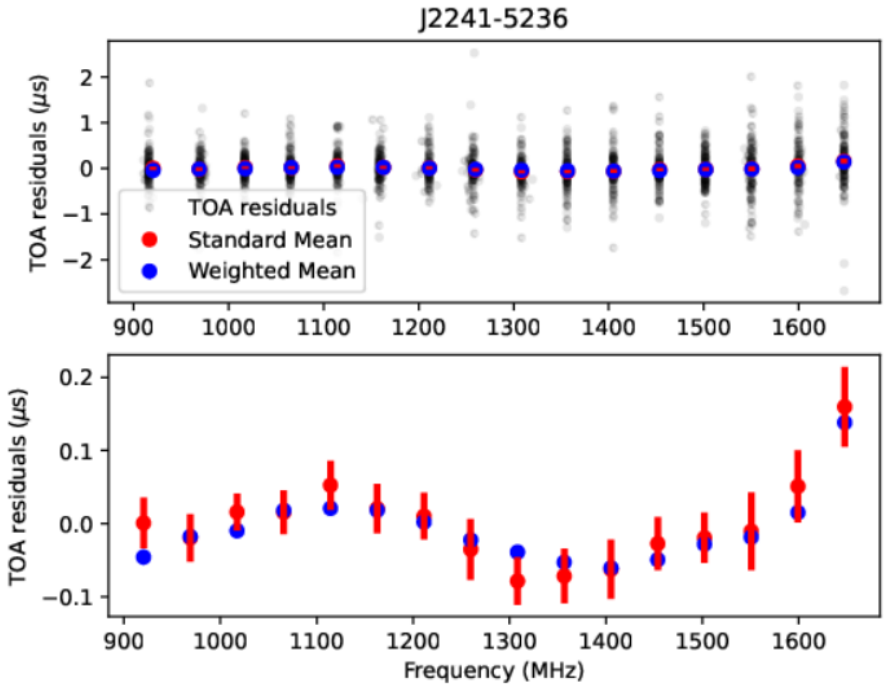

Fig. 2: The 16 sub-band timing residual data for J2241−5236 reveals a frequency-dependent (FD) structure present within the timing residuals. The top plot shows all the ToA residuals as a function of frequency, with the bottom plot zooming in to show the mean and weighted mean of timing residuals for each frequency sub-band. Blue dots show the weighted mean whereas the red points show the mean. Error bars is the standard error in the mean. Some of this frequency-dependent structure could be due to a varying DM over time, but the majority is due to bad template profiles.

2.4 Dispersion Measure Fitting

2.4.1 16-band Data

After frequency-dependent corrections, each observation was fit for DM to reduce the weighted root mean squared (WRMS) residual of the timing residuals for each pulsar. The process applies a DM correction (DMX) to each observation.

The choice to apply both FD corrections and DMX fits had a dramatic effect on the WRMS residuals of the timing residuals, and introduced quadratic artifacts in the timing residuals, whereby ToA residuals at certain frequencies arrived earlier or later than others. For a few pulsars, this lowered the WRMS residual by a significant amount. However, for most pulsars, the WRMS increased, with timing residuals significantly worse.

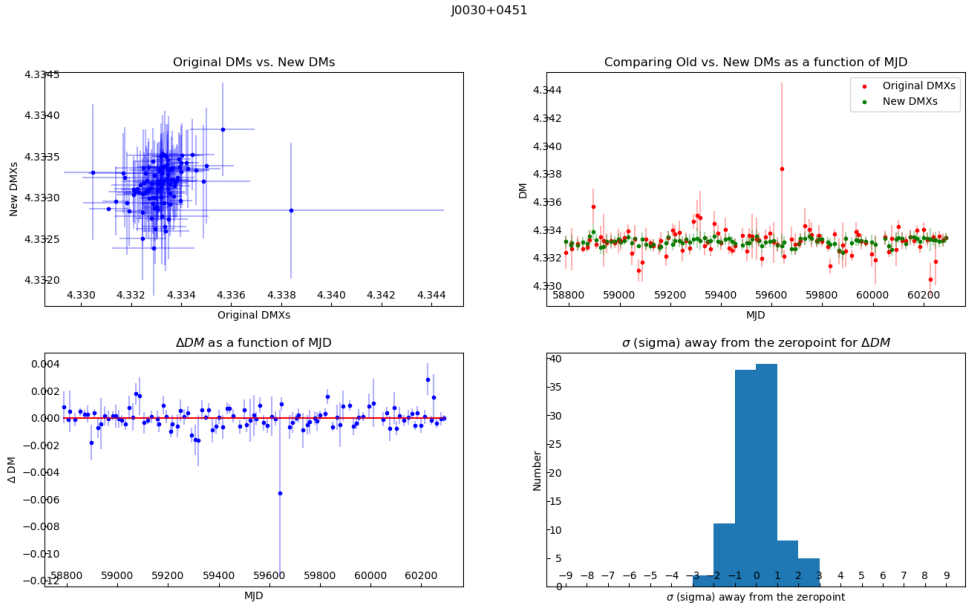

Fig. 3: The process of applying DM corrections to each epoch (DMX fitting) and its lack of any meaningful benefit is shown above. The original DMs were determined by fitting for DM at each epoch. The new DMs were determined by fitting for DMXs across all timing residuals for a given pulsar after fitting DM across each epoch. Top-left: Reveals an uncorrelated spread between the original and new DMs for J0030+0451. Top-right: Shows the difference of the original DMs per epoch and the new DMs per epoch over time and it shows the relatively larger spread of the original DMs. Bottom-left: Determines the change in DM over time, where $\Delta DM = DM_{new} - DM_{original}$ Bottom-right: Number of points $n\,\sigma$ away from the zero-point for the change in DM over time.

This most likely occurred to the covariance between the FD structures and the DM, and the assumption that the DM for each pulsar is correct, when the FD structure could be corrected majorly by a different DM.

These FD corrections may also have an effect on the detection of the gravitational wave background (GWB) due to the effects of the gravitational wave background on ToA residuals as a function of frequency. However, this has yet to be tested using 16-band data.

This process also could have led to over-fitting of the timing residuals for each pulsar, and this results in the loss of... (need to talk to Matt about this.)

2.4.2 32-band Data

Some epochs with $\chi^2 > 3$ required DM fitting to reduce their respective χ^2. This was due to the presence of a $1/\nu^2$ frequency relationship for timing residuals that could be fixed by fitting for DM.

PSR () was removed from our dataset for ()
This final dataset included all arrival times from the 32-band MeerKAT PTA dataset that had been corrected for DM and had been filtered for bad timing residuals. This data was used to search for a correlated signal of the GWB present within the timing residuals.

3 Results

We first measure noise processes present in the final dataset and these noise models were produced by Dr. Matt Miles. Following, we search for correlations between pulsars and hence evidence for gravitational waves present in the final timing residuals. We do this by fitting Hellings-Downs correlations and determine the likelihood of the models using Hellings-Downs correlations are favoured over zero correlations.

Figure 4 shows the correlation we get considering the entire dataset, with an amplitude of $\sim 5 \times 10^{-15}$. This is produced through (number) of pulsar pairs, which were grouped into 15 groups, separated by some angular separation angle ζ. This was detected with a detection statistic of 7.003σ. It can be visualised that the model including a Hellings-Downs correlation fits the spatial correlations better than zero correlation fit.

A portion of the data (timing residuals with $\theta_{\mathrm{SUN,PSR}} \geq 47.5^{\circ}$) where $\theta_{\mathrm{SUN,PSR}}$ is the sun pulsar angle. This produced a stronger spatial correlation, specifically a stronger Hellings-Downs correlation. The amplitude retrieved with this sample of the final dataset reaches approx 8×10^{-15} with a detection significance of 11.7σ. More different amplitudes and their respective detection significances are described further in Discussion.

4 Discussion

4.1 Consistency Checks

The final dataset was thoroughly checked to ensure consistency within the timing residuals, and to assess whether the result (see Figure 4) was from an astrophysical source, or an artificial artefact.

4.1.1 Clock corrections

We first assessed the arrival times, and the mean timing residuals for each observational session (see Figure 6), and their spread around the zero-point. The processing pipeline for MeerKAT applies clock corrections such that the mean timing residuals should be within $1\,\mu s$ of the zero-point, which is largely confirmed through Figure 6.

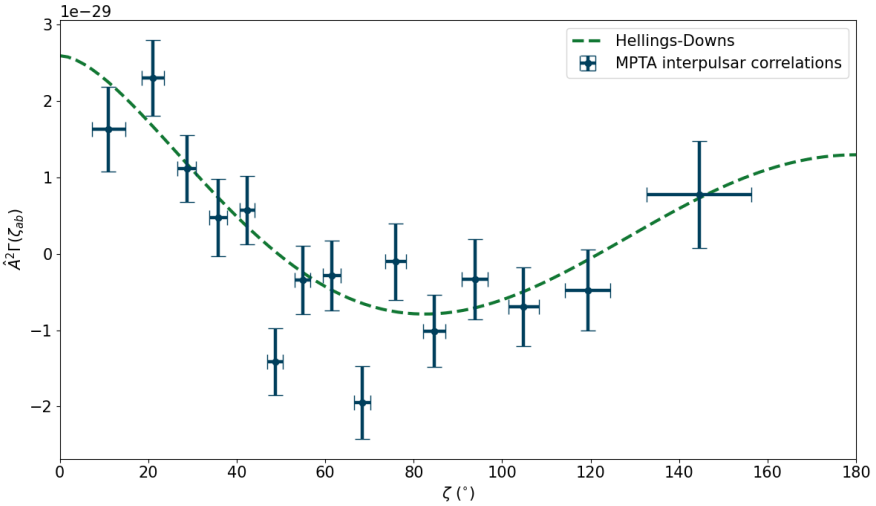

Fig. 4: The spatial correlation as a function of the angular separation angle ζ between timing residuals of pairs of pulsars with an overlapping Hellings-Downs correlation fit. All 32 sub-band ToAs were used in the production of this result.

However, it should be noted that the mean ToA offsets do have very small offsets ($\sim 10^{-21}(units)$), and this results in many of the means being multiple σ away from the zero-point. Some of the mean timing residual offsets reach closer to the $6\,\mu s$, which is due to the low number of pulsars ($n_{\rm PSR} < 3$) in the observation session, resulting in large offsets and also comparatively larger errors.

Overall, Figure 6 shows that the majority of observations have good clock corrections, and hence are accurate in their timing residuals. Figure 7 shows the distribution of mean timing offsets, and the accuracy of the clock corrections and the reliability in the timing residuals is reinforced.

4.1.2 Filtering for DM

Following this, we tested the dataset by searching for Hellings-Downs correlations with filtered samples of the final dataset. One such parameter that was used during this process is DM. Pulsars with a respective DM $DM_{\rm PSR}$ less than some DM cutoff $DM_{\rm cutoff}$ ($DM_{\rm PSR} < DM_{\rm cutoff}$) were filtered. This filtered dataset was used to detect the presence of gravitational waves, and the resultant detection significances are shown below.

4.1.3 Filtering for UTC

We also searched for Hellings-Downs correlations through datasets filtered based on date. We first started by removing the oldest data and then repeated the process, but started with the latest arrival times datasets. The results are as follows.

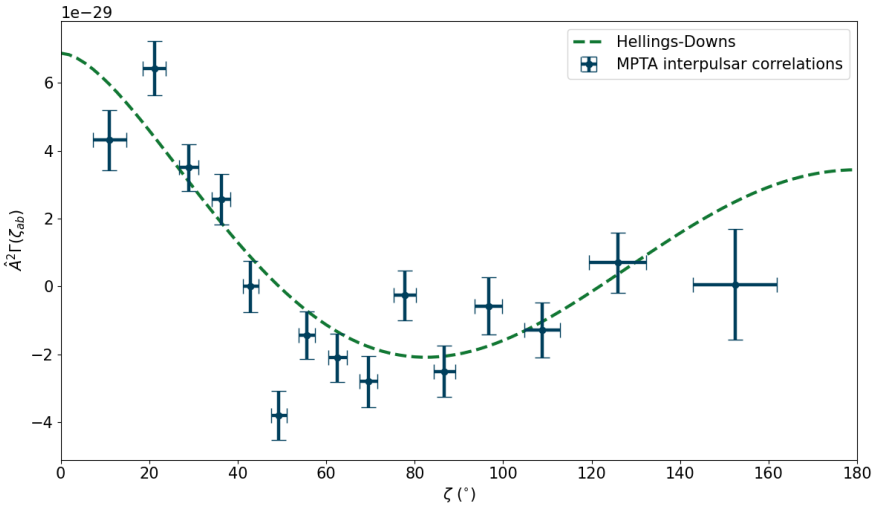

Fig. 5: A filtered dataset where the sun pulsar angle for a given ToA must be greater than 47.5°, which reveals a stronger spatial correlation as a function of angular separation angle ζ. The detection significance is the highest from all filters utilised.

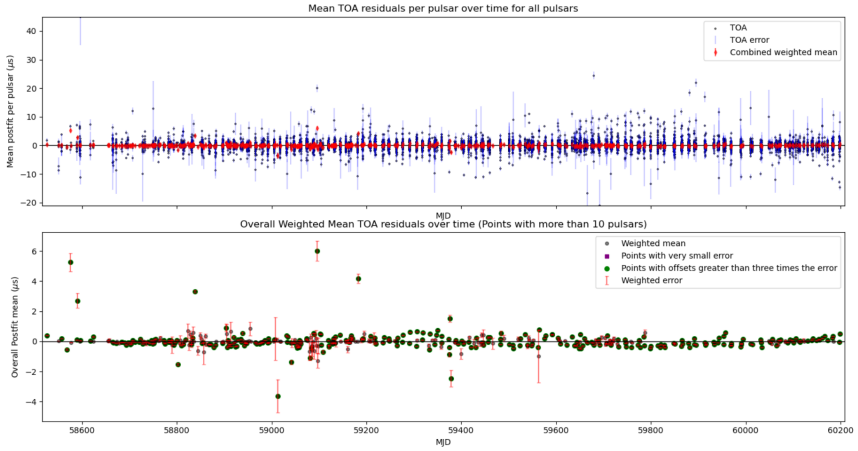

Fig. 6: Mean timing residual offsets for all pulsars on an session-by-session basis. Top: Blue points shows the times of arrival (ToAs) for each observation for each pulsar. Red points shows the mean for each observation. Bottom: A zoomed-in plot of the top plot showing only the means of each of the observation sessions. Points more than 3σ away from the zero-point are coloured green. Besides some large outliers and unusual ToA offset structures as a function of time, this plot shows that the timing residuals are largely accurate.

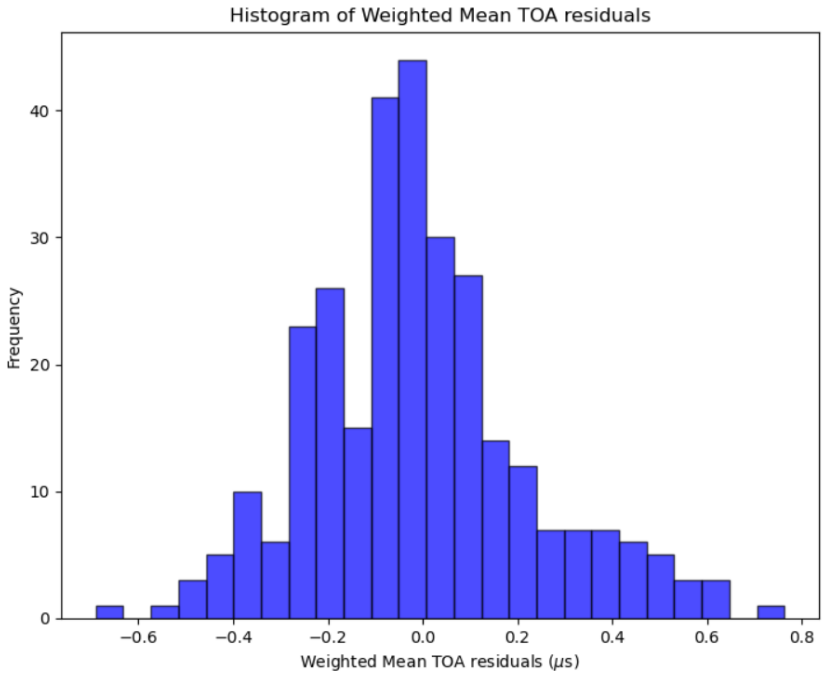

Fig. 7: The distribution of the weighted mean ToA offsets, excluding the means where $n_{\text{points}} < 3$. All of the following means fall with MeerKAT clock correction uncertainties of $1\,\mu s$, and the distribution is approximately symmetrical around the zero-point, leading to high reliability in the timing residuals

4.1.4 Filtering for Sun Pulsar Angle

A similar process was done for filtered datasets, whereby our final dataset was filtered based on the sun pulsar angle. Timing residuals with a sun pulsar angle $\theta_{\text{S,P,PSR}}$ less than some sun pulsar angle cutoff $\theta_{\text{S,P,cutoff}}$ ($\theta_{\text{S,P,PSR}} < \theta_{\text{S,P,cutoff}}$) were removed to produce this filtered dataset. This dataset was then tested for spatial correlations. As previously stated, when $\theta_{\text{S,P,cutoff}} = 47.5°$ (in other words, the filtered dataset had timing residuals where $\theta_{\text{S,P}} \geq 47.5°$), showed the strongest Hellings-Downs correlation, with a signal amplitude of (value) and a detection signifance of approx 11.7σ, the highest thus far. As of now, this is still being actively investigated. The distribution of detection significances as a function of $\theta_{\text{S,P,cutoff}}$ increases up to 47.5°, before significantly decreasing afterwards. This does not match our expectation, where we expected the detection significance to increase slightly, before decreasing gradually as the cutoff is increases.

One possible explanation suggests that the process responsible for fitting models using

Hellings-Downs correlations (enterprise) may lack restrictions as the amount of data decreases (when we increase $\theta_{\mathrm{S,P,cutoff}}$), however, this is currently under investigation.

References

[1] Abbott, B.P., Abbott, R., Abbott, T.D., Abernathy, M.R., Acernese, F., Ackley, K., Adams, C., Adams, T., *et al.*: Observation of gravitational waves from a binary black hole merger. Phys. Rev. Lett. **116**, 061102 (2016) https://doi.org/10.1103/PhysRevLett.116.061102

[2] Abbott, R., Abbott, T.D., Acernese, F., *et al.*: Gwtc-3: Compact binary coalescences observed by ligo and virgo during the second part of the third observing run. Phys. Rev. X **13**, 041039 (2023) https://doi.org/10.1103/PhysRevX.13.041039

[3] Agazie, G., Anumarlapudi, A., Archibald, A.M., Arzoumanian, Z., Baker, P.T., Bécsy, B., Blecha, L., Brazier, A., Brook, P.R., *et al.*: The NANOGrav 15 yr Data Set: Evidence for a Gravitational-wave Background. **951**(1), 8 (2023) https://doi.org/10.3847/2041-8213/acdac6 arXiv:2306.16213 [astro-ph.HE]

[4] Antoniadis, J., Arzoumanian, Z., Babak, S., Bailes, M., Bak-Nielsen, A.-S., Baker, P.T., Bassa, C.G., Bécsy, B., Berthereau, A., Bonetti, *et al.*: The International Pulsar Timing Array second data release: Search for an isotropic gravitational wave background. Monthly Notices of the Royal Astronomical Society **510**(4), 4873–4887 (2022) https://doi.org/10.1093/mnras/stab3418 https://academic.oup.com/mnras/article-pdf/510/4/4873/42242297/stab3418.pdf

[5] Bailes, M., Berger, B.K., Brady, P.R., Branchesi, M., Danzmann, K., Evans, M., Holley-Bockelmann, K., Iyer, B.R., Kajita, T., *et al.*: Gravitational-wave physics and astronomy in the 2020s and 2030s. Nature Reviews Physics **3**(5), 344–366 (2021) https://doi.org/10.1038/s42254-021-00303-8

[6] Begelman, M.C., Blandford, R.D., Rees, M.J.: Massive black hole binaries in active galactic nuclei. Nature **287**(5780), 307–309 (1980) https://doi.org/10.1038/287307a0

[7] EPTA Collaboration, Antoniadis, J., Babak, S., Bak Nielsen, A.-S., Bassa, C. G., Berthereau, A., Bonetti, M., *et al.*: The second data release from the european pulsar timing array - i. the dataset and timing analysis. AA **678**, 48 (2023) https://doi.org/10.1051/0004-6361/202346841

[8] Einstein, A.: Die Feldgleichungen der Gravitation. Sitzungsberichte der Koniglich Preußischen Akademie der Wissenschaften, 844–847 (1915)

[9] Foster, R.S., Backer, D.C.: Constructing a Pulsar Timing Array. **361**, 300 (1990) https://doi.org/10.1086/169195

[10] Hellings, R.W., Downs, G.S.: Upper limits on the isotropic gravitational radiation background from pulsar timing analysis. **265**, 39–42 (1983) https://doi.org/10.1086/183954

[11] Hulse, R.A., Taylor, J.H.: Discovery of a pulsar in a binary system. **195**, 51–53 (1975) https://doi.org/10.1086/181708

[12] Johnston, S., Lorimer, D.R., Harrison, P.A., Bailes, M., Lynet, A.G., Bell, J.F., Kaspi, V.M., Manchester, R.N., D'Amico, N., Nleastrol, L., Shengzhen, J.: Discovery of a very bright, nearby binary millisecond pulsar. Nature **361**(6413), 613–615 (1993) https://doi.org/10.1038/361613a0

[13] Lee, K.J., Wex, N., Kramer, M., Stappers, B.W., Bassa, C.G., Janssen, G.H., Karuppusamy, R., Smits, R.: Gravitational wave astronomy of single sources with a pulsar timing array. Monthly Notices of the Royal Astronomical Society **414**(4), 3251–3264 (2011) https://doi.org/10.1111/j.1365-2966.2011.18622.x https://academic.oup.com/mnras/article-pdf/414/4/3251/18708099/mnras0414-3251.pdf

[14] Morello, V., Barr, E.D., Cooper, S., Bailes, M., Bates, S., Bhat, N.D.R., Burgay, M., Burke-Spolaor, S., Cameron, A.D., Champion, D.J., Eatough, R.P., *et al.*: The High Time Resolution Universe survey – XIV. Discovery of 23 pulsars through GPU-accelerated reprocessing. Monthly Notices of the Royal Astronomical Society **483**(3), 3673–3685 (2018) https://doi.org/10.1093/mnras/sty3328 https://academic.oup.com/mnras/article-pdf/483/3/3673/27299713/sty3328.pdf

[15] Milosavljević, M., Merritt, D.: Long-term evolution of massive black hole binaries. The Astrophysical Journal **596**(2), 860 (2003) https://doi.org/10.1086/378086

[16] McConnell, N.J., Ma, C.-P.: Revisiting the Scaling Relations of Black Hole Masses and Host Galaxy Properties. **764**(2), 184 (2013) https://doi.org/10.1088/0004-637X/764/2/184 arXiv:1211.2816 [astro-ph.CO]

[17] Miles, M.T., Shannon, R.M., Bailes, M., Reardon, D.J., Keith, M.J., Cameron, A.D., Parthasarathy, A., Shamohammadi, M., *et al.*: The MeerKAT Pulsar Timing Array: first data release. Monthly Notices of the Royal Astronomical Society **519**(3), 3976–3991 (2022) https://doi.org/10.1093/mnras/stac3644 https://academic.oup.com/mnras/article-pdf/519/3/3976/48617501/stac3644.pdf

[18] Magorrian, J., Tremaine, S., Richstone, D., Bender, R., Bower, G., Dressler, A., Faber, S.M., Gebhardt, K., Green, R., Grillmair, C., Kormendy, J., Lauer, T.: The demography of massive dark objects in galaxy centers. The Astronomical Journal **115**(6), 2285 (1998) https://doi.org/10.1086/300353

[19] Narayan, R.: The Physics of Pulsar Scintillation. Philosophical Transactions of

the Royal Society of London Series A **341**(1660), 151–165 (1992) https://doi.org/10.1098/rsta.1992.0090

[20] Reardon, D.J., Coles, W.A., Bailes, M., Bhat, N.D.R., Dai, S., Hobbs, G.B., Kerr, M., Manchester, R.N., *et al.*: Precision orbital dynamics from interstellar scintillation arcs for psr j0437–4715. The Astrophysical Journal **904**(2), 104 (2020) https://doi.org/10.3847/1538-4357/abbd40

[21] Rickett, B.J.: Radio propagation through the turbulent interstellar plasma. **28**, 561–605 (1990) https://doi.org/10.1146/annurev.aa.28.090190.003021

[22] Reardon, D.J., Zic, A., Shannon, R.M., Hobbs, G.B., Bailes, M., Di Marco, V., Kapur, A., Rogers, A.F., Thrane, E., Askew, J., *et al.*: Search for an Isotropic Gravitational-wave Background with the Parkes Pulsar Timing Array. **951**(1), 6 (2023) https://doi.org/10.3847/2041-8213/acdd02 arXiv:2306.16215 [astro-ph.HE]

[23] Sazhin, M.V.: Opportunities for detecting ultralong gravitational waves. **22**, 36–38 (1978)

[24] Taylor, J.H., Fowler, L.A., McCulloch, P.M.: Measurements of general relativistic effects in the binary pulsar J1913+16. **277**(5696), 437–440 (1979) https://doi.org/10.1038/277437a0

Appendices

A Steps

A.1 Obtaining the data

The 16 channel data was obtained from Swinburne supercomputer directory */fred/oz005/users/nswainst/meerpipe_testing_outputs*. An environment variable **MEERPIPE** was defined to refer to this directory. There is one directory per pulsar. This data was used to develop a pipeline to process and clean the data based on set criteria.
Later, the 32 channel data from */fred/oz002/dreardon/mk_gw/pipeline/djr_final_final_final* was used to do the gravitational wave analysis. The csh script *32chan.csh* was used to copy the data to the project directory.
The project directory used was */fred/oz002/users/mbailes/astral/timing/*. An environment variable called **MATTHEW** was created to refer to the directory */fred/oz002/users/mbailes/*. The following command was used to concatenate the *.tim* files and copy them to the new directory:

```
cd $MEERPIPE
foreach pulsar (‘cat $MATTHEW.... | awk etc)
  mkdir $MATTHEW/timing/$pulsar
  cat 2*/?/1284/timing/*tim >> $MATTHEW/timing/$pulsar/${pulsar}.tim
  cp ‘find . -name ${pulsar}.par | tail -1‘ $MATTHEW/timing/$pulsar
end
```

All scripts can be found in the */fred/oz002/users/mbailes/astral/bin* directory.

A.2 Cleaning the data

A.2.1 Using the 16 channel data

By manual inspection, using tempo2, bad epochs were identified, where the data points had clear irregularities. Error and SNR thresholds were then identified to get rid of most points with large ToA errors. The points were deleted and the data was refitted to create new *.par* and *.tim* files.
The error thresholds and bad epochs (for individual pulsars) were recorded in the spreadsheet *toa_error_bad_dates.csv*. Epochs that showed problems across all pulsars were recorded in *removal_dates.dat*.
Using these criteria, the script *cleanData.py* was run on the original data to double check the quality of the culling. An example of the command used to run the script is:

```
python3 CleanData.py ../Pars/toa_error_bad_dates.csv
```

A.2.2 Using the 32 channel data

The script *clean32ChanData.py* was used to clean the 32 channel data. The epochs that were obtained from the 16 channel data, a SNR cutoff of 6, a ToA error cutoff of 10, and a minimum observation length requirement of 128.0 s, were used to remove points in the 32 channel data *.tim* files. This was done to limit the effect of jitter on the observation. In both cases the new *.tim* files were created with the name format *JNAME.auto.tim*.

The χ^2 was calculated for each observation and each pulsar using *chi2r.csh* and recorded in the file *JNAME.auto.CHI2R.csv*. By modelling the expected distribution of the χ^2, and comparing it to the χ^2 of the data, the appropriate cutoffs for the χ^2 value per data point was determined to be 3.6.

Finally the script *gwbprep.csh* was run on the remaining data to delete points that had χ^2 values higher than the 3.6 cutoff. Observations that had fewer than 7 points points and a number of bands fewer than 5 were also removed. The new *.tim* files were labeled *JNAME.gwb.tim*.

The *.tim* files for *J1843-1448* had to be culled manually using separate criteria as it did not have enough points that passed the initial round of culling.

The *gwb* prepped *.tim* and *JNAME.matt.par* files could at last be copied to the directory */fred/oz002/users/mbailes/astral/GWB/OpStat/partim* and the names were changed to *JNAME.tim* and *JNAME.par*.

A.3 Searching for gravitational waves

The directory *fred/oz002/users/mbailes/astral/GWB/OpStat/* was mirrored from Daniel's similar directory and the apptainer shell was installed and run using the following commands:

```
ml apptainer
cd $MATTHEW/astral/bin
apptainer shell-B /fred,$HOME apptainer.sif
cd ../GWB/OpStat
```

The script *os_matt_fix.py* was used to run a search for gravitational waves. The results were read out on the screen and the plot of the data compared to the Hellings-Downs curve was saved as *MPTA_OS.png* in the OpStat directory using the Apptainer shell. To preserve the original, most unbiased, dataset, the *partim/* directory was copied to *astral0/*.

Next the dataset was culled based on various parameters to investigate their influence on the optimal statistic. All of the following scripts saved their Hellings-Downs curves in the *.../OpStat/pngs* directory and statistics in the *.../OpStat/stats* directory.

A.3.1 Varying the start and end dates

First, the dependence of the optimal statistic on the start and end date of the data was determined. The script *delete_date_tim_new.py* was created to automatically create a new *partim/_date* directory to vary the start date of the data. To

run it, add a start cutoff date (yyyy-mm-dd) as the first argument. Then to run a GWB search on these newly created files, the *os_matt_fix.py* script was copied to *os_matt_fix_dateranges_new.py* and was run using the same date as before as the first argument.
Similarly, the scripts *delete_date_tim_reverse_new.py* and *os_matt_fix_dateranges_reverse_new.py* were created and used in the same way to create *partim* directories that contain all data up to a certain cutoff date and run a search on it.

A.3.2 Varying the DM cutoffs

Next the pulsars with a specific cutoff DM were removed from the data set and a GWB search was run. The script *dm_cutoff_gwb.py*[1] was used to create the new *patim* directories and *os_matt_fix_dmcut_date.py* was used to run the gravitational search. For both scripts the desired DM-cutoff was input as the first argument. A batch job was used to run for multiple DM-cutoffs.

A.3.3 Culling based on Sun-Pulsar angle

Finally, observations were removed based on their Sun-pulsar angle. The script *sun_psr_angle_cutoff_gwb.py*[2] was used to create the new directory and copy the qualifying files. *os_matt_fix_sun_psr_angle.py* was then used to run the GWB search on the corresponding files. The Sun-pulsar angle was added as the first argument for both scripts.

B - Python Scripts

[1] dm_cutoff_gwb.py only uses data from 2020-01-01, it does not include data from 2019
[2] sun_psr_angle_cutoff_gwb.py uses all the data including 2019